J. of Basic Sciences, Cheju Nat'l Univ.
20(1), 99~104, 2007

기초과학연구 제주대학교
20(1), 99~104, 2007

Phase Shift Analysis of ^{10,11}C + p Elastic Scattering

Yong Joo Kim*
Department of Physics, Cheju National University, Jeju 690-756

Differential cross sections of elastic scattering for ^{10}C + p system at E_{lab}/A = 45.3 MeV/nucleon and ^{11}C + p system at E_{lab}/A = 40.6 MeV/nucleon have been analyzed using the eikonal approximation and first-order eikonal model, respectively. The calculated results lead to a good agreement with the experimental data. A Fuller decomposition of the scattering amplitudes have shown that the elastic cross sections are dominated by the far-side amplitude. The strong real potential is required to describe the large angle behavior of the cross section which is dominated by the far-side component of the scattering amplitude.

I. INTRODUCTION

The most commonly studied process (experimentally and theoretically) in the scattering problem is that of elastic scattering. Heavy-ions elastic scattering has been used as the starting point to understand more complicated scattering mechanism. The outcome of elastic scattering data analysis generally is required to begin studies of other reaction process. There have been much theoretical efforts [1-8] to analyze the heavy ion elastic scattering. The heavy-ion elastic scattering is generally dominated by the strong absorption, which the implication that the data are only sensitive to the surface of the interaction region. Therefore, the optical potential required to describe the measurements is not uniquely determined. However, the angular distributions of light heavy-ions elastic scattering have shown the presence of strong refractive effects which are interpreted as the dominance of contributions from the far side of the scattering center. The refractive phenomena seen in the elastic scattering angular distributions of light heavy-ions provide a unique source of information on the heavy-ion interaction potentials at small internuclear distance.

Over the last decades, eikonal model is useful and convenient tools to describe the heavy-ion elastic scattering. A number of studies [9-12] have been made to describe elastic scattering processes between heavy-ions within the framework of the eikonal model. The phase shifts in the eikonal model are derived from the integral equation by further approximation the WKB results. The use of the distance of closest approach as an effective impact parameter in the eikonal formula provides a simple and efficient way to study heavy-ion scattering at relatively low energies [12]. In the early work of Cha and Kim [13], we have presented the first- and second-order corrections to the zeroth-order eikonal phase shifts for heavy-ion elastic scatterings based on Coulomb trajectories of colliding nuclei and it has been applied satisfactorily to the ^{16}O + ^{40}Ca and ^{16}O + ^{90}Zr systems at E_{lab}=1503 MeV. The elastic scatterings of ^{16}O + ^{16}O system at E_{lab} = 350 and 480 MeV have been analyzed within the framework of second-order Coulomb-modified eikonal model using the tangential velocity at the distance of closest approach [14].

Since the advent of secondary radioactive beams far from stability, many nuclear physicists have paid attention to studies of exotic nuclei [15-21]. The neutron rich nuclei with large neutron-to-proton ratio, such as ^{6,8}He [17], ^{11}Li [15, 16] and ^{18,20,22}O [18, 21] has been studied extensively. Recently, to probe the ground state and transition densities, the neutron-deficient nuclei elastic and inelastic scattering on a proton target were measured in inverse kinematics for the unstable ^{10}C and ^{11}C nuclei [20] at 45.3 and 40.6 MeV/nucleon, respectively. These neutron-deficient nuclei elastic cross section data are compared to the optical model calculations performed within the framework of microscopic nucleus-nucleon Jeukenne-Lejeune-Mahaux potential approach, and direct structure information (matter rms radii, neutron moment for ^{10}C) was extracted.

It is interesting to apply the eikonal model analysis for the neutron-deficient nuclei elastic scattering on proton. In this paper, we will calculate elastic scattering cross sections for ^{10}C + p system at E_{lab}/A = 45.3 MeV/nucleon and ^{11}C + p system at E_{lab}/A = 40.6 MeV/nucleon, respectively, by using the phase shift analysis based on eikonal model, and compare theoretical results with the experimental data. In the following section, the relevant details of eikonal model are given. In section III, we present the results and conclusions of our analysis.

II. THEORY

The elastic differential scattering cross section is given by the following equation:

$$\frac{d\sigma}{d\Omega} = |f(\theta)|^2. \tag{1}$$

Ignoring the spin-orbit effects, we write the elastic scattering amplitude $f(\theta)$ as

$$f(\theta) = f_R(\theta) + \frac{1}{ik}\sum_{L=0}^{\infty}(L+\frac{1}{2})\exp(2i\sigma_L)(S_L^N - 1)P_L(\cos\theta), \tag{2}$$

*Electronic address: yjkim@cheju.ac.kr

where $f_R(\theta)$ is the usual Rutherford scattering amplitude and σ_L the Coulomb phase shift. The nuclear S-matrix elements S_L^N in this equation can be expressed by the nuclear phase shift δ_L as

$$S_L^N = e^{2i\delta_L}. \tag{3}$$

If there is a single turning point in the radial Schrödinger equation, a first-order WKB expression for the nuclear elastic phase shifts δ_L, taking into account the deflection effect due to Coulomb field, can be written as [10]

$$\delta_L = \int_{r_t}^{\infty} k_L(r)\,dr \; - \; \int_{r_c}^{\infty} k_c(r)\,dr, \tag{4}$$

where r_t and r_c are the turning points corresponding to the local wave numbers $k_L(r)$ and $k_c(r)$ given by

$$k_L(r) = k\Big[1 - \Big(\frac{2\eta}{kr} + \frac{L(L+1)}{k^2r^2} + \frac{U_N(r)}{E}\Big)\Big]^{1/2}, \tag{5}$$

$$k_c(r) = k\Big[1 - \Big(\frac{2\eta}{kr} + \frac{L(L+1)}{k^2r^2}\Big)\Big]^{1/2}, \tag{6}$$

where η is the Sommerfeld parameter, and $U_N(r)$ the nuclear potential. If we consider the nuclear potential as a perturbation, the nuclear phase shift including up to the first-order correction term can be written as

$$\begin{aligned}\delta_L(r_c) \;=\; & -\frac{\mu}{\hbar^2 k}\int_{r_c}^{\infty}\frac{rU_N(r)}{(r^2-r_c^2)^{1/2}}dr \\ & -\frac{\mu^2}{2\hbar^4k^3}\int_{r_c}^{\infty}\frac{r^3U_N^2(r)}{(r^2-r_c^2)^{3/2}}dr,\end{aligned} \tag{7}$$

where $r = \sqrt{r_c^2+z^2}$, and r_c is the Coulomb distance of closest approach given by

$$r_c = \frac{1}{k}\Big\{\eta + \Big[\eta^2 + L(L+1)\Big]^{1/2}\Big\}. \tag{8}$$

The first term in Eq.(7) is the ordinary Coulomb-modified eikonal phase shift, while the second term is the first-order corrections correspond to noneikonal effects. The nuclear phase shift $\delta_L(r_c)$ in Eq.(7) can be rewritten as following

$$\begin{aligned}\delta_L(r_c) \;=\; & -\frac{\mu}{\hbar^2 k}\int_0^{\infty}U_N(r)dz \\ & -\frac{\mu^2}{2\hbar^4k^3}\Big(1 + r_c\frac{d}{dr_c}\Big)\int_0^{\infty}U_N^2(r)\,dz.\end{aligned} \tag{9}$$

The first-order eikonal correction term of the phase shift, $\delta_L^1(r_c)$ in Eq.(9), can further be expressed as following

$$\delta_L^1(r_c) = -\frac{\mu^2}{\hbar^4k^3}\int_0^{\infty}\Big[U_N^2(r) + rU_N(r)\frac{dU_N(r)}{dr}\Big]\,dz\,. \tag{10}$$

The closed expression of the effective phase shift function including up to the first-order correction term may be written as

$$\delta_L(r_c) = -\frac{\mu}{\hbar^2 k}\int_0^{\infty}U_{\rm eff}(r)\,dz\,, \tag{11}$$

where $U_{\rm eff}(r)$ is the effective optical potential given by

$$U_{\rm eff}(r) = U_N(r)\Big\{1 + \frac{\mu}{\hbar^2k^2}\Big[U_N(r) + r\frac{dU_N(r)}{dr}\Big]\Big\}. \tag{12}$$

We can see that the phase shift calculation including non-eikonal corrections up to the first-order is equivalent to a zeroth-order calculation with effective potential $U_{\rm eff}(r)$. The nuclear potential $U_N(r)$ in this work will be taken as the usual optical Woods-Saxon form given by

$$U_N(r) = -\frac{V_0}{1+e^{(r-R_v)/a_v}} - i\frac{W_0}{1+e^{(r-R_w)/a_w}}, \tag{13}$$

with $R_{v,w} = r_{v,w} \times A_p^{1/3}$.

The removal of probability current in elastic scattering is related to the fact that processes other than elastic ones may occur in a nuclear collision, which absorb some of this current. A quantitative measure for the absorption is provided by the reaction or absorption cross section. The total reaction cross section is defined as

$$\sigma_R = \frac{\pi}{k^2}\sum_{L=0}^{\infty}(1 - |S_L^N|^2). \tag{14}$$

This relationship established a link between the scattering and the reaction cross sections.

III. RESULTS AND CONCLUSIONS

TABLE I: Parameters of the fitted Woods-Saxon potential by using the eikonal approximation (Cal.1) and first-order eikonal model (Cal.2) for the elastic scatterings of ^{10}C + p system at $E_{\rm lab}$/A= 45.3 MeV/nucleon.

	V_0 (MeV)	r_v (fm)	a_v (fm)	W_0 (MeV)	r_w (fm)	a_w (fm)	σ_R (mb)	χ^2/N
Cal.1	31.8	1.45	0.49	9.8	1.52	0.27	262	4.90
Cal.2	41.5	1.29	0.51	20.8	1.13	0.32	268	4.23

We have applied the eikonal model to calculate the elastic differential cross sections for ^{10,11}C + p at $E_{\rm lab}/A$=45.3 and 40.6 MeV/nucleon, respectively. Table I and II show the parameters of the fitted Woods-Saxon potential. The six potential parameters are adjusted so as to minimize the χ^2/N given by

$$\chi^2/N = \frac{1}{N}\sum_{i=0}^{N}\Big[\frac{\sigma_{exp}^i - \sigma_{cal}^i}{\Delta\sigma_{exp}^i}\Big]^2. \tag{15}$$

TABLE II: Parameters of the fitted Woods-Saxon potential by using the eikonal approximation (Cal.1) and first-order eikonal model (Cal.2) for the elastic scatterings of ^{11}C + p system at E_{lab}/A= 40.6 MeV/nucleon.

	V_0 (MeV)	r_v (fm)	a_v (fm)	W_0 (MeV)	r_w (fm)	a_w (fm)	σ_R (mb)	χ^2/N
Cal.1	32.9	1.50	0.34	8.8	1.44	0.41	272	5.57
Cal.2	48.4	1.25	0.48	17.2	1.08	0.37	272	3.59

In Eq.(15),$\sigma^i_{exp}(\sigma^i_{cal})$ and $\Delta\sigma^i_{exp}$ are the experimental (calculated) cross sections and uncertainties, respectively, and N is the number of data used in the fitting. The calculated results of the differential cross sections for the elastic scattering of ^{10}C + p system at E_{lab}/A= 45.3 MeV/nucleon and ^{11}C + p system at E_{lab}/A= 40.6 MeV/nucleon, respectively, are presented in figures 1 and 2 together with the observed data [20]. In these figures, the dashed curves are the best calculated cross sections using the eikonal approximation, while the solid curves are those obtained when first-order eikonal model are used. Clearly, there are excellent agreements between the calculated results and the experimental data [20]. The reasonable χ^2/N values are obtained in the ^{10}C + p at E_{lab}/A=45.3 MeV/nucleon and ^{11}C + p at E_{lab}/A=40.6 MeV/nucleon, respectively, as listed in Table I and II. If we judge from χ^2/N point of view, the calculated results of first-order eikonal model give some better agreement with the observed data compared to one of eikonal approximation, as shown in tables I and II. The values of χ^2/N decrease explicitly in the calculated results using the first-order eikonal model compared to the ones with eikonal approximation. In table I and II, one can find that two calculations give the nearly same reaction cross sections due to using best fitted potential parameters not using the same potential parameters, although there is small difference in ^{10}C + p system at E_{lab}/A=45.3 MeV /nucleon.

More insight into the structure of the angular distribution can be provided by the representation of the elastic scattering amplitude in terms of the near-side and far-side components. The near-side amplitude represents a contribution from the wave deflected in the direction of θ on the near-side of the scattering center and the far-side amplitude represents a contribution from the wave travelling from in opposite side of the scattering center to the same angle θ. The near- and the far-side decompositions of the scattering amplitudes due to the Fuller's formalism [22] are obtained from

$$f(\theta) = f_N(\theta) + f_F(\theta), \qquad (16)$$

where

$$f_{N(F)}(\theta) = f_{R_{N(F)}}(\theta) + \frac{i}{2k}\sum_{L=0}^{\infty}(2L+1)\exp(2i\sigma_L) \times(1 - S_L^N)Q_L^{(\mp)}(\cos\theta). \qquad (17)$$

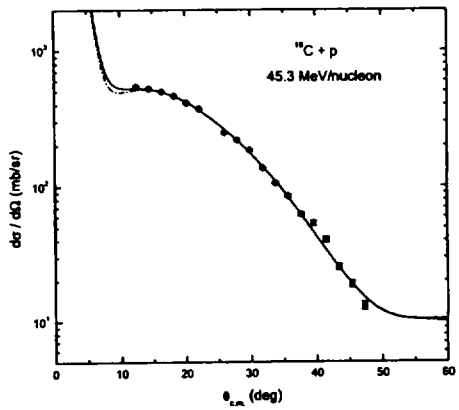

FIG. 1: Elastic scattering angular distributions for ^{10}C + p system at E_{lab}/A= 45.3 MeV/nucleon. The solid circles denote the observed data taken from Jouanne *et al.* [20]. The solid curves are the calculated results using the first-order eikonal model, while the dashed curve is the result from the eikonal approximation.

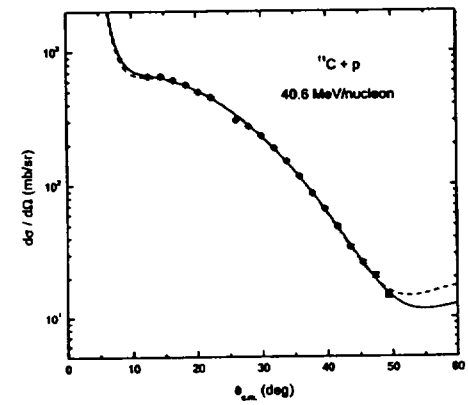

FIG. 2: Elastic scattering angular distributions for ^{11}C + p system at E_{lab}/A= 40.6 MeV/nucleon. The solid circles denote the observed data taken from Jouanne *et al.* [20]. The solid curves are the calculated results using the first-order eikonal model, while the dashed curve is the result from the eikonal approximation.

Here, f_{R_N} and f_{R_F} are the near- and far-side Rutherford amplitudes, respectively, and $Q_L^{(\mp)}$ are linear combinations of Legendre functions of the first and the second kind according to

$$Q_L^{(\mp)}(\cos\theta) = \frac{1}{2}\Big[P_L(\cos\theta) \pm i\frac{2}{\pi}Q_L(\cos\theta)\Big]. \qquad (18)$$

The contributions of the near- and far-side components to

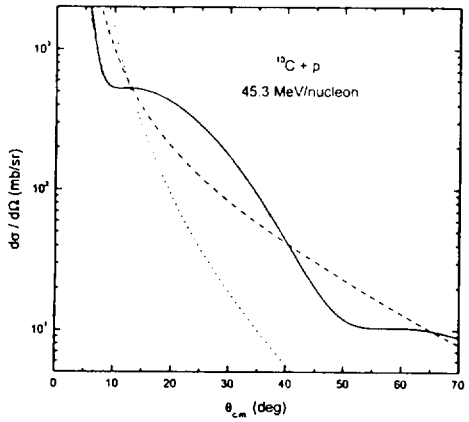

FIG. 3: Differential cross section (solid curve), near-side contribution (dotted curve), and far-side contribution (dashed curve) following the Fuller's formalism [22] from the first-order eikonal model for ^{10}C + p system at E_{lab}/A= 45.3 MeV/nucleon.

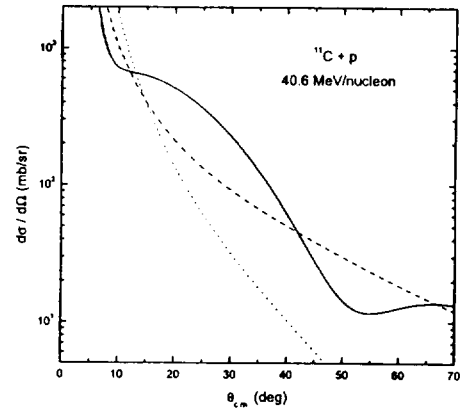

FIG. 4: Differential cross section (solid curve), near-side contribution (dotted curve), and far-side contribution (dashed curve) following the Fuller's formalism [22] from the first-order eikonal model for ^{11}C + p system at E_{lab}/A= 40.6 MeV/nucleon.

the elastic scattering cross sections using the first-order eikonal model are shown in Fig. 3 (^{10}C + p system) and Fig. 4 (^{11}C + p system) along with the total differential cross sections. The total differential cross section is not just a sum of the near- and far-side cross sections but contains the very small interference between the near- and far-side amplitudes as shown in Fig. 3 and Fig. 4 . In both cases, the near-side amplitude are very small compared to the far-side one over the whole angle. Due to the smallness of the near-side components, we can find that angular distributions for ^{10}C + p system at E_{lab}/A= 45.3 MeV/nucleon and ^{11}C + p system at E_{lab}/A= 40.6 MeV/nucleon, respectively, show very weak oscillations.

In order to represent the partial wave contributions to the cross sections in terms of orbital angular momentum L, we plot in Fig. 5 the real and imaginary parts of the term $S = \frac{1}{i}(L + \frac{1}{2})e^{2i\sigma_L}(S_L^N - 1)$. The first-order eikonal model results of ^{10}C + p system at E_{lab}/A= 45.3 MeV/nucleon and ^{11}C + p system at E_{lab}/A= 40.6 MeV/nucleon are shown in the left and right panel, respectively. In this figure, we can see that two parts of S play an only important role in the small angular momentum zone less than L = 8. For both system, the imaginary part (S_{Im}) dominates compared to real one (S_{Re}).

The real and imaginary parts of the optical potential for eikonal approximation and first-order eikonal model calculations, respectively, are displayed in Fig. 6. The results of ^{10}C + p system at E_{lab}/A= 45.3 MeV/nucleon are shown in left panel, and ^{11}C + p system at E_{lab}/A= 40.6 MeV/nucleon presented in the right panel, respectively. In both calculations, the strongly real and weakly imaginary optical potentials are found to be essential to

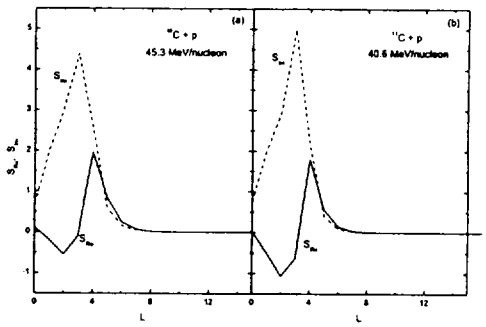

FIG. 5: Real (S_{Re}) and imaginary (S_{Im}) parts of $S = \frac{1}{i}(L + \frac{1}{2})e^{2i\sigma_L}(S_L^N - 1)$ using the first-order eikonal model for (a) ^{10}C + p system at E_{lab}/A= 45.3 MeV/nucleon and (b) ^{11}C + p system at E_{lab}/A= 40.6 MeV/nucleon plotted versus orbital angular momentum L.

describe the experimental data. In the small r region, the imaginary potential is small compared with the real potential. This implies deep elastic interpenetration of the target and projectile. The deep real potential deflect internal trajectories to large negative angles, therefore, is required to describe the large angle behavior of cross sections corresponding to far-side scattering. As a result, the cross section becomes sensitive to the value of the real potential in the central region.

In conclusion, we have analyzed the elastic scattering of ^{10}C + p system at E_{lab}/A= 45.3 MeV/nucleon and ^{11}C + p system at E_{lab}/A= 40.6 MeV/nucleon us-

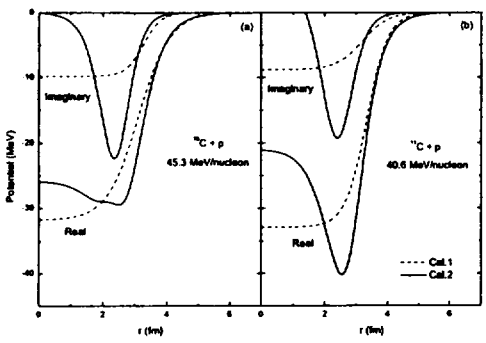

FIG. 6: Real and imaginary potentials for (a) $^{10}C + p$ system at $E_{lab}/A = 45.3$ MeV/nucleon and (b) $^{11}C + p$ system at $E_{lab}/A = 40.6$ MeV/nucleon. The solid and dashed curves represent the results from the first-order eikonal model and eikonal approximation, respectively.

ing the first-order eikonal model and eikonal approximation, respectively. The predicted results have been found to reproduce satisfactorily the differential cross sections, and a comparison with experimental data has given excellent agreement over the whole angular range. We can find that the agreements between the first-order eikonal model results and experimental data are some better compared to the eikonal approximation result. A Fuller decomposition of the scattering amplitudes into the near- and far-side components have shown that the cross sections are dominated by the far-side amplitude. The strongly real and weakly imaginary optical potentials were required to reproduce the $^{10,11}C + p$ elastic scattering data and these potential features make it possible to interpenetrate each other between the projectile and target. As a result, the cross section becomes sensitive to the value of the real potential at small r value. We have seen that the deep real potential is essential to describe the large angle behavior of the cross section which is dominated by the far-side component of the scattering amplitude.

[1] M. Buenerd, *et al.*, Nucl. Phys. **A424**, 313 (1984).
[2] M. C. Mermaz, Z. Phys. **A321**, 613 (1985).
[3] M. E. Brandan, Phys. Rev. Lett. **60**, 784 (1988).
[4] E. Stiliaris, *et al.*, Phys. Lett. **223**, 291 (1989).
[5] D. T. Khoa, *et al.*, Phys. Rev. Lett. **74**, 34 (1995).
[6] G. Bartnitzky, *et al.*, Phys. Lett. B **365**, 23 (1996).
[7] M. P. Nicoli, *et al.*, Phys. Rev. **C60** 064608 (1999).
[8] Dao T. Khoa, *et al.*, Nucl. Phys. **A672**, 387 (2000).
[9] T. W. Donnelly, *et al.*, Nucl. Phys. Nucl. Phys. **A232**, 355 (1974).
[10] C. K. Chan, *et al.*, Phys. Rev. C **24**, 2035 (1981).
[11] F. Carstoiu, *et al.* Phys. Rev. C **48** 830 (1993).
[12] C. E. Aguiar, *et al.*, Phys. Rev. **C56**, 1511 (1997).
[13] M. H. Cha and Y. J. Kim, Phys. Rev. **C51**, 212 (1995).
[14] Y. J. Kim and M. H. Cha, Int. J. Mod. Phys. **E12**, 479 (2003).
[15] I. Tanihata, *et al.*, Phys. Lett. **B287**, 307 (1992).
[16] C. B. Moon, *et al.*, Phys. Lett. **B297**, 39 (1992).
[17] A. A. Korsheninnikov, *et al.*, Nucl. Phys.. **A617**, 45 (1997).
[18] E. Khan, *et al.*, Phys. Lett. **B490**, 45 (2000).
[19] A. Lagoyannis, *et al.*, Phys. Lett. **B518**, 27 (2001).
[20] C. Jouanne, *et al.*, Phys. Rev. **C72**, 014308 (2005).
[21] E. Becheva, *et al.*, Phys. Rev. Lett **96**, 012501 (2006).
[22] R. C. Fuller, Phys. Rev. **C12**, 1561 (1975).

$^{10,11}C+p$ 탄성산란에 대한 위상이동 분석

김 용 주

제주대학교 물리학과, 제주 690-756

E_{lab}/A = 45.3 MeV/nucleon 인 $^{10}C + p$ 계와 E_{lab}/A = 40.6 MeV/nucleon 인 $^{11}C + p$ 계의 탄성산란에 대한 미분단면적을 Eikonal 근사와 제1차 Eikonal 모형을 이용하여 분석하였다. 계산결과는 실험값과 좋은 일치를 보여주었다. 산란진폭에 대한 Fuller의 분해를 통하여 원측 진폭이 탄성산란단면적에서 주된 역할을 함을 알 수 있었다. 산란진폭의 원측 성분에 의해 지배를 받는 큰 산란각에서의 산란단면적을 기술하기 위해서는 강한 실수 퍼텐셜이 요구되었다.